The Direct Method in Strapdown Airborne Gravimetry – a Review

Felix Johann, David Becker, Matthias Becker, René Forsberg and Majid Kadir

Summary

This paper reviews various aspects of the direct method in airborne gravimetry, using a strapdown inertial measurement unit (IMU) and GNSS. The direct method (also referred to as "accelerometry approach" or "cascaded approach") is a cascaded two-step approach: inertial accelerations are computed from GNSS positions using numerical differentiation in the first step, which are then removed from IMU specific force measurements in the second step. The transformation of strapdown measurements into the navigation frame requires the knowledge of the vehicle's attitude, which is commonly computed using a commercial IMU/GNSS strapdown navigation software. In contrast, the indirect method (also referred to as "inertial navigation approach" or "one-step approach") combines all available measurements (GNSS positions and IMU measurements) in a single Kalman-Filter, which is, however, more difficult to implement and requires a substantial tuning of the filter.

A comparison of both approaches based on real campaign data indicates the overall quality of the two approaches being on a par. The accuracy achieved is 0.6 mGal (after line adjustment) and 1.3 mGal (without adjustment) at flight altitude, with a spatial resolution of about 6 km (half-wavelength). These results demonstrate for the first time that both processing approaches can achieve gravity disturbances at the same level of accuracy.

This paper discusses the fundamentals of the direct method, addressing readers who are striving for their own implementation. The various corrections and data processing aspects are presented in detail as well as a standard evaluation scheme.

Zusammenfassung

Dieser Artikel befasst sich mit verschiedenen Aspekten der Fluggravimetrie unter Verwendung eines Strapdown-Inertialen-Messsystems (IMU) und GNSS. Die Direkte Methode (auch „Beschleunigungsansatz" oder „Mehr-Schritt-Verfahren" genannt) ist ein zweistufiges Verfahren: Im ersten Schritt werden aus GNSS-Positionen mittels numerischer Differenziation inertiale Beschleunigungen bestimmt, die dann von den IMU-Beobachtungen der spezifischen Kraft entfernt werden. Zur Transformation der Strapdown-Messungen in Navigationskoordinaten wird die Orientierung des Flugzeugs benötigt, die sich mit einer kommerziellen IMU/GNSS-Strapdown-Navigationssoftware bestimmen lässt. Im Gegensatz dazu werden bei der Indirekten Methode alle verfügbaren Messungen (GNSS-Positionen und IMU-Beobachtungen) in einem gemeinsamen Kalman-Filter kombiniert, was einen höheren Implementierungsaufwand und Filtertuning erforderlich macht.

Ein Vergleich beider Methoden anhand der Auswertung einer realen Messkampagne ergibt für beide Ansätze eine Gesamtgenauigkeit mit einer Standardabweichung von 0,6 mGal (nach Kreuzungspunktjustierung) und 1,3 mGal (ohne Justierung) in Flughöhe bei einer Auflösung von etwa 6 km (halbe Wellenlänge). Damit wird erstmals gezeigt, dass mit beiden Prozessierungsansätzen Ergebnisse auf dem gleichen Genauigkeitsniveau erhalten werden können.

Der Artikel ist insbesondere an Leser gerichtet, die die Grundlagen der Direkten Methode verstehen möchten, möglicherweise um eine eigene Implementierung vorzunehmen. Es wird in die Grundlagen des Ansatzes eingeführt und verschiedene Korrektionen und Aspekte der Datenprozessierung werden im Detail betrachtet. Eine Standardmethode zur Qualitätsanalyse wird kurz erläutert.

Keywords: Airborne gravimetry, strapdown, IMU, GNSS, gravity

1 Introduction

Airborne gravimetry can be seen as an intermediate gravity determination method between satellite and terrestrial gravimetry in terms of accuracy and resolution. The first test flights applying airborne gravimetry have been undertaken in the early 1960s using a horizontally stabilized spring gravimeter (Nettleton et al. 1960). At that time, the positioning accuracy proved to be the limiting factor in airborne gravimetry. Due to the rise of the Global Positioning System (GPS) in the 1990s, airborne gravimetry was successfully conducted in many campaigns, e.g. Brozena et al. (1997).

Since the 1980s, the use of inertial measurement units (IMU) in airborne gravimetry was subject of research as an alternative to spring gravimeters. An IMU commonly consists of a triad of gyroscopes and accelerometers each. This newer type of gravimetry is also called "strapdown airborne gravimetry" since a horizontally stabilized platform is not required. Further advantages of strapdown airborne gravimetry are the lower space, weight and power consumption. In addition, the full 3-D gravity vector is determinable (vector gravimetry), the sensitivity to turbulences and flight altitude changes is reduced and costs and maintenance requirements are lowered (Becker 2016). It was shown that accuracies on a similar level compared to "classic" airborne gravimetry using stable-platform gravimeters are achievable if the impact of strong IMU drifts is reduced by removing a linear drift

from the gravity estimates (Glennie et al. 2000). Furthermore, recent research has demonstrated that the majority of accelerometer drifts can be compensated using IMU calibration methods (Becker 2016). In fact, it was shown that a simple thermal lab calibration of just the *vertical* accelerometer was already able to eliminate the bulk of drifts (Becker et al. 2015b).

In strapdown airborne gravimetry, mainly two processing approaches exist (Jekeli and Garcia 1997). When applying the so-called *direct* method, gravity is determined by forming the difference of kinematic acceleration and accelerometer measurements. In the *indirect* method, all available IMU and GNSS measurements are integrated in a single Kalman filter. The separation of specific force and gravity is done indirectly using GNSS positions rather than accelerations, hence the method's name.

The following sections will give some basics of strapdown gravimetry including the main differences between the two processing methods. This paper shows the direct method of strapdown gravimetry in detail, presenting an elaborate algorithm including all required corrections.

Section 2 provides some fundamentals of strapdown airborne gravimetry. The differences between the two methods are briefly discussed in Section 3. The algorithm of the direct method is then shown in detail in sections 4 and 5, including filtering and all corrections that need to be applied.

A meaningful comparison among different airborne gravimetry campaigns is difficult, since flight parameters, topography and the actual gravity field characteristics are different. In addition, the quality assessment methods are not standardized. In this paper, a crossover residual analysis is implemented, which is introduced in section 6.

The data sets presented in this paper have been evaluated using both the direct and the indirect method, allowing a direct comparison of the two methods (section 7).

2 Fundamentals of Strapdown Airborne Gravimetry

In strapdown airborne gravimetry, the accelerometers of a strapdown IMU are used to measure the specific force $\boldsymbol{f}$ being the difference of the vehicle's kinematic acceleration $\ddot{\boldsymbol{r}}$ and gravity $\boldsymbol{g}$. The geometric position $\boldsymbol{r}$ is usually obtained by GNSS (Global Navigation Satellite Systems) observations and corresponding processing methods. In order to determine gravity, the equation can be suitably solved as follows (Kwon and Jekeli 2001):

$$\boldsymbol{f}^i = \ddot{\boldsymbol{r}}^i - \boldsymbol{g}^i \;\Leftrightarrow\; \boldsymbol{g}^i = \ddot{\boldsymbol{r}}^i - \boldsymbol{f}^i . \tag{1}$$

The latter equation is valid only if the quantities are given in a non-rotating inertial frame, indicated with the superscript *i*. Two additional coordinate frames, body frame *b* and navigation frame *n*, are required. While the body frame's orientation (e.g. front, right/starboard, down) is fixed to the IMU's attitude, the navigation frame's orientation (e.g. north, east, down) is defined by geodetic north, the normal to the ellipsoid and the east axis completing the right-handed orthogonal set. Gravity is commonly related to the navigation frame *n*, whereas in strapdown gravimetry the specific force measurement is referenced to the body frame *b*. The latter is then transformed into the *n*-frame by means of the gyroscope measurements. As the origins of body and navigation frame coincide by definition, the frame transformation is fully defined by a 3-by-3 rotation matrix $\boldsymbol{C}_b^n$.

Instead of gravity itself, the much smaller gravity *disturbance* $\boldsymbol{\delta g}^n$ is the more common output quantity in airborne gravimetry. It is defined as the difference of gravity $\boldsymbol{g}^n$ and normal gravity $\boldsymbol{\gamma}^n$ at the measurement point (Becker and Hehl 2012). In order to account for Coriolis and centrifugal forces, the Eötvös correction $\boldsymbol{\delta g}_{\text{eot}}^n$ needs to be applied (Wei and Schwarz 1998):

$$\boldsymbol{\delta g}^n = \ddot{\boldsymbol{r}}^n - \boldsymbol{C}_b^n \boldsymbol{f}^b + \boldsymbol{\delta g}_{\text{eot}}^n - \boldsymbol{\gamma}^n . \tag{2}$$

In order to obtain $\boldsymbol{\delta g}_{\text{eot}}^n$, the skew-symmetric matrices $\boldsymbol{\Omega}_{ie}^n, \boldsymbol{\Omega}_{en}^n$ of the Earth rotation and the transport rate must be known. The first matrix contains the angular velocity of the Earth rotation with respect to the inertial frame; the second matrix describes the rotation of the moving navigation frame with respect to the Earth-fixed frame (Groves 2013). The Eötvös correction is then given as (Wei and Schwarz 1998)

$$\boldsymbol{\delta g}_{\text{eot}}^n = \left(2\boldsymbol{\Omega}_{ie}^n + \boldsymbol{\Omega}_{en}^n\right) \cdot \dot{\boldsymbol{r}}^n , \tag{3}$$

with velocity vector $\dot{\boldsymbol{r}}^n$. The first term quantifies the Coriolis acceleration; the second term quantifies the centrifugal acceleration due to the movement of an object relative to Earth. Note, that the centrifugal acceleration due to the Earth rotation is already included in normal gravity.

In their vectorial form, equations (2) and (3) allow the determination of both the horizontal and vertical components of the gravity disturbance. In scalar gravimetry, only the down component

$$\delta g_D = g_D - \gamma = \ddot{r}_D - f_D - \delta g_{\text{eot}} - \gamma \tag{4}$$

of equation (2) is being used.

3 Indirect versus Direct Method

This section describes the main ideas of the indirect and the direct processing methods in strapdown airborne gravimetry. The algorithm of the direct method will be

shown in detail including required corrections in sections 4 and 5.

In the literature, there are various alternative terms for the "indirect" method as introduced by Jekeli (2001). It has also been called "inertial navigation approach" (Ayres-Sampaio et al. 2015) or "traditional way" (Kwon and Jekeli 2001). Here, IMU observations are integrated with respect to time and the gravity disturbance is obtained from the comparison of IMU-predicted position and GNSS position. All observations, i. e. IMU and GNSS data, are processed in a single extended Kalman filter (EKF), which is why the method is also called "one-step approach" (Becker 2016). Fig. 1 illustrates the workflow of the indirect method, which has to be executed epoch wise.

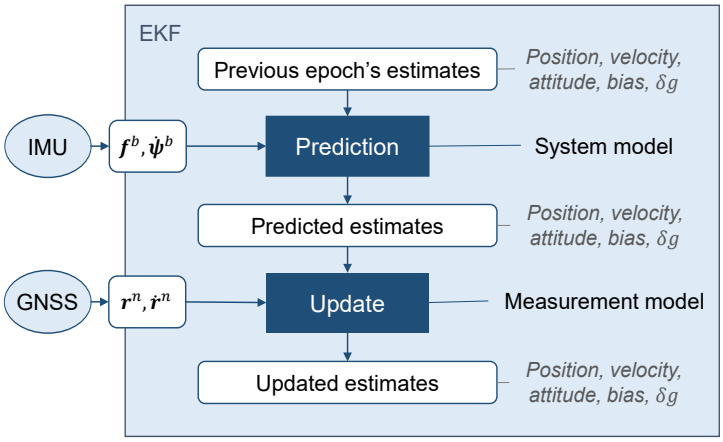

Fig. 1: Schematic flow chart of the loosely coupled indirect method in strapdown airborne gravimetry using an extended Kalman filter (EKF)

The Kalman filter is based on an inertial navigation filter, but besides position, velocity, orientation and sensor biases, the state vector is supplemented by one or three gravity states, for scalar or vector gravimetry, respectively. In the prediction step, inertial navigation equations are used to propagate the last epoch's state estimates to the current epoch using IMU accelerometer and gyroscope observations (acceleration $\boldsymbol{f}^b$ and angular velocity $\dot{\boldsymbol{\psi}}^b$) that are integrated with respect to time (Ayres-Sampaio et al. 2015). The predicted estimates are then corrected in the measurement update step using GNSS pseudorange and phase measurements (*tightly* coupled approach), or using pre-processed GNSS position $\boldsymbol{r}^n$ and velocity $\dot{\boldsymbol{r}}^n$ solutions (*loosely* coupled approach). Since, in general, satellite coverage is excellent in airborne gravimetry, the simpler loosely coupled implementation is sufficient in most cases. Deviant from the flow chart in Fig. 1, Kalman filters in the indirect method are often implemented using an error state space formulation in order to improve numerical stability. Further details on Kalman filters used for inertial navigation and airborne gravimetry can be found in Groves (2013), Becker (2016), and others.

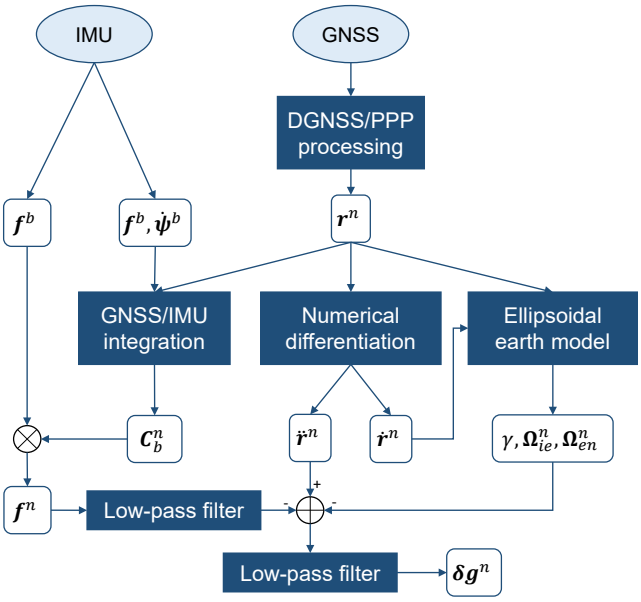

Fig. 2: Flow chart of the direct method implemented in the scope of this work

The direct method has also been called "accelerometry approach" (Kwon and Jekeli 2001, Ayres-Sampaio et al. 2015), since the IMU accelerations are compared directly to accelerations derived from GNSS data. The direct method is realized in form of a "cascaded approach" (Becker 2016) and requires several consecutive processing steps. A possible implementation is visualized in Fig. 2 and introduced in this section. A detailed algorithm will be presented in section 4, clarifying the quantities shown in Fig. 2. As an alternative to the procedure shown here, the direct method can also be implemented as an one-step Kalman filter approach where position and velocity are not included in the state vector (Jekeli 2001).

Like in the loosely coupled variant of the indirect method, the cascaded algorithm starts with the determination of GNSS positions, which are then numerically differentiated twice in order to obtain kinematic accelerations. IMU accelerometer and gyroscope measurements are used in combination with the GNSS solutions to precisely estimate the aircraft's attitude (GNSS/IMU integration). The IMU acceleration measurements are transformed from body to navigation frame utilizing these attitude estimates. With GNSS position and velocity at hand, normal gravity, Earth rotation rate and transport rate can be computed. Finally, gravity disturbances are computed using equation (2) or (4). Due to strong high-frequency noise, the results need to be low-pass filtered. By comparing the gravity disturbance with known values at the start and landing airports, bias and linear drift are removed from the data.

In the scope of this paper, biases and drifts are determined solely for the resulting gravity disturbance. In the procedure presented in Glennie and Schwarz (1999), accelerometer biases and drifts are estimated by the IMU/GNSS Kalman filter and then applied to the original specific force measurements.

An advantage of the indirect method is that it is based on a known optimal estimation procedure used in inertial navigation, the Kalman filter. Moreover, the method has been argued to be more rigorous since all data is introduced to a single optimal estimator (Becker 2016).

The indirect method also has disadvantages. Because inertial navigation and observation equations are not linear, the indirect method does not provide a truly optimal estimation and approximate initial estimates for attitude are required. The stochastic model of the Kalman filter needs to be tuned carefully. Small changes in filter parameters can significantly affect the results in a way which is difficult to understand. Therefore, the direct method is less arcane (Jekeli 2001) and easier to implement, especially, if a proven external pre-processing software is used for the GNSS/IMU integration.

4 Algorithm of the Direct Method

The algorithm used in the scope of this work is illustrated in the flow chart in Fig. 2 and will be discussed in the following. Input quantities for equation (2) will be determined stepwise.

4.1 GNSS Processing and GNSS/IMU Integration

First, a geodetic GNSS processing method analyzing two frequency phase observations needs to be applied in order to obtain precise positions subsequently used as input data for the numerical differentiation. Typically, baselines to known GNSS reference stations are evaluated using Phase-Differential GNSS (PDGNSS). Recent studies showed that Precise Point Positioning (PPP) using precise satellite orbits and clocks determined in post-processing can give results on a par with PDGNSS depending on the set-up and the length of baselines to reference stations in PDGNSS (Becker 2016). Furthermore, the processing approaches MKin-VADASE ("Modified Kinematic Variometric Approach for Displacements Analysis Stand-alone Engine") and POP ("Precise Orbit Positioning") have been reported to be adequate alternatives applicable to airborne gravimetry (Salazar et al. 2011, Zhang et al. 2017, Li et al. 2019).

Precise attitude information is obtained by performing a GNSS/IMU integration. The transformation between body and navigation frame is expressed by three Euler angles: roll, pitch and yaw. These angles can be transformed into a 3-by-3 rotation matrix or, alternatively, into a quaternion, and vice versa. Both the GNSS processing and the GNSS/IMU integration can be performed using standard navigation software.

4.2 Numerical Differentiation of GNSS Positions

Having GNSS positions $\boldsymbol{r}$ at hand, velocity $\dot{\boldsymbol{r}}$ and acceleration $\ddot{\boldsymbol{r}}$ are computed by numerical differentiation.

Several numerical differentiation methods using the primary difference quotient, the central difference quotient or cubic interpolation polynomials (Schwarz and Köckler 2011) have been tested within the scope of this work. No significant effect on the gravity results was observed. The simplest way to obtain the first derivative $f'(t)$ of a discrete function $f(t)$ with step size Δt is the use of the primary difference quotient. If this approach is applied, epochs will be shifted by half a time step: At the middle position t_M between two function values y_0, y_1, the first derivative can be approximated as

$$f'(t_M) \approx \frac{\Delta y_{0,1}}{\Delta t_{0,1}} = \frac{y_1 - y_0}{\Delta t}, \quad \text{with} \quad t_M = \frac{t_0 + t_1}{2}. \tag{5}$$

If the position is given as geodetic longitude λ and latitude ϕ, a transformation into meters is required which can be applied after the first numerical differentiation. Considering the radii of curvature R_n, R_e and the ellipsoidal height h, velocity $\dot{\boldsymbol{r}}$ can be transformed into the navigation frame n (North, East, Down) as follows (Hwang et al. 2006):

$$\dot{\boldsymbol{r}}^n = \begin{pmatrix} \dot{r}_N \\ \dot{r}_E \\ \dot{r}_D \end{pmatrix} = \begin{pmatrix} (R_n + h)\cdot\dot{\phi} \\ (R_e + h)\cdot\cos(\phi)\cdot\dot{\lambda} \\ -\dot{h} \end{pmatrix}, \quad \ddot{\boldsymbol{r}}^n = \begin{pmatrix} \ddot{r}_N \\ \ddot{r}_E \\ \ddot{r}_D \end{pmatrix}. \tag{6}$$

4.3 IMU Pre-processing

If attitude information is obtained from the GNSS/IMU integration in the form of three Euler angles, these angles are transformed into a rotation matrix for each epoch. The rotation matrix $\boldsymbol{C}_n^b$ describes the rotation transforming coordinates from the navigation to the body frame. The reverse rotation from the body to the navigation frame is obtained by an inversion of the matrix. Since the matrix is orthogonal, the inversion can be replaced by the numerically simpler transposition $\boldsymbol{C}_b^n = \left(\boldsymbol{C}_n^b\right)^{-1} = \left(\boldsymbol{C}_n^b\right)^T$. Details on the setup of rotation matrices can be found, for example, in Groves (2013).

Pre-processing steps have to be applied to the IMU's specific force measurements. Since, in strapdown gravimetry, the IMU is tied to the body frame, the acceleration observations $\boldsymbol{f}^b$ obtained in the body frame need to be transformed to the navigation frame. If the origins of both frames coincide by definition, the specific force $\boldsymbol{f}^n$ in the navigation frame is obtained by applying the rotation matrix $\boldsymbol{C}_b^n$.

The IMU data rate is commonly higher than the available GNSS data rate. Furthermore, the IMU epochs may not coincide with GNSS epochs. Therefore, the specific

force measurements need to be interpolated to the GNSS epochs. Since IMU observations are typically affected by high frequency noise, the specific force measurements need to be smoothed using a low-pass filter *before* the interpolation can be applied reasonably.

4.4 Quantities obtained with GNSS Solutions

The remaining input quantities for equation (2) are evaluated at each GNSS epoch using GNSS positions and their first derivatives as computed by equation (6). With the scalar Earth rotation rate set to $\omega_{ie} = 7{,}292115 \cdot 10^{-5}\,\mathrm{s}^{-1}$ (Moritz 1980), the skew-symmetric matrix $\boldsymbol{\Omega}_{ie}^{n} = \left[\boldsymbol{\omega}_{ie}^{n}\times\right]$ of the Earth rotation rate $\boldsymbol{\omega}_{ie}^{n}$ is given as

$$\boldsymbol{\Omega}_{ie}^{n} = \omega_{ie}\begin{pmatrix} 0 & \sin(\phi) & 0 \\ -\sin(\phi) & 0 & -\cos(\phi) \\ 0 & \cos(\phi) & 0 \end{pmatrix}, \tag{7}$$

where ϕ is the geodetic latitude (Groves 2013). $[\boldsymbol{v}\times]$ denotes the skew-symmetric matrix of a vector $\boldsymbol{v}$. In addition to the geodetic latitude, the ellipsoidal height h, the radii of curvature R_n, R_e, and the GNSS derived velocity $\dot{\boldsymbol{r}}$ from equation (6) are needed to express the skew-symmetric matrix $\boldsymbol{\Omega}_{en}^{n} = \left[\boldsymbol{\omega}_{en}^{n}\times\right]$ of the transport rate $\boldsymbol{\omega}_{en}^{n}$ as

$$\boldsymbol{\Omega}_{en}^{n} = \begin{pmatrix} 0 & \dfrac{\dot{r}_E \tan(\phi)}{R_e + h} & -\dfrac{\dot{r}_N}{R_n + h} \\ -\dfrac{\dot{r}_E \tan(\phi)}{R_e + h} & 0 & -\dfrac{\dot{r}_E}{R_e + h} \\ \dfrac{\dot{r}_N}{R_n + h} & \dfrac{\dot{r}_E}{R_e + h} & 0 \end{pmatrix}. \tag{8}$$

Equations for normal gravity $\boldsymbol{\gamma}^{n}$ can be found, e.g., in Torge and Müller (2012), equations 4.72b, 4.78, 4.79. The east component of $\boldsymbol{\gamma}^{n}$ is exactly zero due to the rotational symmetry of the normal gravity field.

4.5 Gravity Disturbance Determination

Eventually, the aforementioned quantities are combined based on equations (2) and (3) to determine the gravity disturbance

$$\delta \boldsymbol{g}^{n} = \ddot{\boldsymbol{r}}^{n} - \boldsymbol{f}^{n} + \left(2\boldsymbol{\Omega}_{ie}^{n} + \boldsymbol{\Omega}_{en}^{n}\right)\cdot \dot{\boldsymbol{r}}^{n} - \boldsymbol{\gamma}^{n}. \tag{9}$$

The high-frequency sensor noise of both IMU specific force measurements and GNSS-derived kinematic vehicle accelerations can be larger than the wanted gravity precision level by several orders of magnitude. Such short wavelength noise is commonly attenuated by applying a low pass filter to the right side of equation (9), enabling the extraction of the longer wavelength gravity signal. Common cutoff filter lengths are 100 s or more, depending on parameters such as flight altitude, topography and aircraft velocity.

5 Additional Corrections

This section introduces additional corrections, which are applied to the resulting gravity disturbance estimates as given by equation (9). Depending on the instrument, flight and set-up characteristics, these corrections may improve the accuracy level significantly.

5.1 Bias and Drift Determination

Since accelerometer measurements can be subject to significant biases and drifts, a correction based on a linear drift approximation is shown in the following. Either, the correction is applied to the IMU acceleration data (Glennie and Schwarz 1999) or to the obtained gravity disturbance. The latter strategy will be presented in this paper.

If ground gravity values at the airports are known from terrestrial gravimetry, the vertical gravity biases κ_i before and after the flight can be easily computed with

$$\kappa_i = \delta g_{D,i} - \delta g_{D,\mathrm{ref},i} = \delta g_{D,i} - (g_{\mathrm{ref},i} - \gamma_{\mathrm{ref},i}), \tag{10}$$

with vertical gravity disturbance $\delta g_{D,i}$ as given by equation (9), ground reference gravity disturbance $\delta g_{D,\mathrm{ref},i}$, ground reference gravity $g_{\mathrm{ref},i}$ and normal gravity $\gamma_{\mathrm{ref},i}$.

A short distance between the aircraft parking position and the ground reference point of tens of meters is usually negligible due to the small variation of the gravity disturbance field. To improve the bias accuracy, δg_D should be determined as the mean values of all observations during the static periods before and after the flight.

Typically, no gravity reference values with sufficient accuracy are available for a bias update during the flight. Therefore, between the ground readings before and after the flight, only the *linear* fraction of the drift can be determined, whereas the non-linear components are inestimable. For any epoch t during the flight, the bias $\kappa(t)$ can be approximated based on the biases κ_1, κ_2 at the reference epochs t_1, t_2 before and after the flight as

$$\kappa(t) = \kappa_1 + \frac{t - t_1}{t_2 - t_1}\left(\kappa_2 - \kappa_1\right). \tag{11}$$

The bias and trend-free vertical gravity disturbance is obtained by subtracting $\kappa(t)$ from the vertical gravity disturbance as given by equation (9). Note that no frame transformation is required here as the linear drift removal is done in the navigation frame.

5.2 Lever Arm between IMU and GNSS Antenna

The positions of the IMU's center of observations, i.e. the body frame origin, and the GNSS antenna phase center are different. The lever arm vector $\boldsymbol{l}^b$ comprises the coordinates of the GNSS antenna in the body frame. Assuming a constant aircraft attitude, the lever arm will not affect the gravity estimates given by equation (9), as the time derivatives of a constant position offset are zero. However, if the attitude varies due to flight maneuvers and turbulence, a correction is required.

Note that the lever arm also needs to be taken into consideration when computing normal gravity at the IMU center of observations, rather than the GNSS antenna position.

The lever arm should be determined precisely in the body frame, e.g. by photogrammetric or tachymetric measurements, or by incorporating respective states in the GNSS/IMU integration model. For each GNSS epoch, the lever arm needs to be transformed to the navigation frame using the rotation matrix $\boldsymbol{C}_b^n$. The position of the IMU center of observations $\boldsymbol{r}^n$ used in equation (6) is then given as the difference of the GNSS antenna position $\boldsymbol{r}_{\mathrm{GNSS}}^n$ and the lever arm $\boldsymbol{l}^n$ expressed in the navigation frame:

$$\boldsymbol{r}^n = \boldsymbol{r}_{\mathrm{GNSS}}^n - \boldsymbol{l}^n . \tag{12}$$

Note that the lever arm may need to be transformed into units of geodetic coordinates to evaluate this equation in practice.

5.3 Thermal IMU Calibration

IMUs commonly show a sensor-temperature dependent behavior. In order to avoid such errors, a temperature-stabilized housing may be used. However, such a housing adds more space, weight and power consumption and therefore weakens some of the major advantages of strapdown gravimetry compared to platform-stabilized gravimetry.

Instead of their mitigation, the thermal effects can be corrected applying a temperature calibration. Becker (2016) presented several calibration strategies. Using an iMAR RQH IMU (IMAR Navigation 2012), significant improvements could be achieved even with a simple warm-up calibration of the vertical accelerometer (Becker et al. 2015b). This approach is applied in this work.

To determine the parameters of the warm-up calibration, the vertical accelerometer readings and the interior sensor temperature have been observed under static conditions (Becker et al. 2015b). Over several consecutive days, the IMU was turned on at room temperature and the sensor readings were logged during the sensor's warm-up period. By averaging over the several runs, a correction function for an internal temperature range of about 20 °C to 45 °C could be obtained, with a total variation of 40 mGal. Applying this correction function to airborne data enabled a gravity accuracy level of 1 mGal.

Since the error $\varepsilon_{\mathrm{IMU},D}$ obtained by the correction function is referred to the down axis of the IMU, the correction has to be applied to the original sensor readings (before their transformation into the n-frame). The corrected acceleration component $f_{D,\mathrm{cor}}^b$ is obtained by subtracting the error from the uncorrected value f_D^b:

$$f_{D,\mathrm{cor}}^b = f_D^b - \varepsilon_{\mathrm{IMU},D} . \tag{13}$$

5.4 Empirical Heading-Dependent Correction

With the same measurement system, Becker (2016) reported a heading-dependent error in the vertical component of the gravity estimates. Since the origin of this effect has not been identified yet, a purely empiric correction is determined, which needs to be applied for each GNSS epoch.

The absolute value of the error is maximal on flight sections along a meridian; it is zero for motions at constant latitude. Therefore, the correction model is based on the north component $\dot{r}_N$ of the aircraft velocity. The correction amplitude c is determined empirically by minimizing the crossover differences for a particular campaign (cf. section 6). The corrected vertical gravity disturbance $\delta g_{D,\mathrm{cor}}$ is obtained by subtracting the error ε_ψ from the uncorrected value δg_D as follows:

$$\varepsilon_\psi = -c\,\dot{r}_N , \quad \delta g_{D,\mathrm{cor}} = \delta g_D - \varepsilon_\psi . \tag{14}$$

The correction should be applied to the gravity disturbance estimates as given by equation (9).

The cause for the observed effect is unclear. Since the correction depends on velocity with respect to the fixed Earth, it is conceivable that the Eötvös correction in equation (3) does not completely remove all effects that occur due to the coordinate frames moving with respect to each other. On the other hand, there might as well be an uncorrected instrumental error (Becker 2016) or a modeling/approximation error.

The empirical estimates of c among various campaigns also suggested a latitude dependency, with c being larger at the Equator and decreasing towards the poles.

5.5 Restriction to Flight Lines

In the following, approximately straight parts of a flight trajectory will be called "flight lines" or just "lines". In contrast to some classical platform-stabilized gravimeters, in strapdown airborne gravimetry, the gravity dis-

turbance can be determined not just along the flight lines but also during maneuvers.

However, the scalar gravity estimation accuracy is lower during maneuvers, e. g. during the turns, because of horizontal accelerations propagating into the vertical gravity estimates by means of small attitude errors (Becker et al. 2015a). For this reason, we limit our quality assessment to flight line data. For a better comparability of quality measures among various campaigns/publications, it is important to state exactly, which sections of the flights were excluded from the quality assessment, if any.

6 Crossover Analysis

In airborne gravimetry, several quality assessment strategies exist. In the scope of this work, a crossover analysis is performed for quality assessment and network adjustment purposes.

6.1 Quality Assessment

Expecting gravity disturbance estimates at an accuracy level of 1 mGal, temporal changes of the Earth's gravity field are neglected: The impact of tidal and loading effects, deformation of the Earth's crust or varying centrifugal acceleration due to Earth rotation, precession and nutation is well below 1 mGal (Becker 2016).

In general, there are two types of quality assessment: An internal assessment is based just on the airborne gravimetry estimates, while an external assessment takes into account external information, like upward-continued ground gravity points. For an internal quality assessment, two or more redundant and uncorrelated airborne measurements are required at (or close to) the same point. One strategy is to repeat a particular flight line and define equidistant points along that line. In a second strategy, which is evaluated in this paper, the main survey lines are typically orthogonally crossed by control lines.

Note that the gravity field for two repeated traversals of a flight line is maximally correlated. Therefore, when using longer low pass filter lengths, the agreement will necessarily increase, potentially leading to a too optimistic quality estimate. At a crossover point of orthogonally intersecting lines, the along-track gravity field variations are uncorrelated, enabling the determination of an optimal along-track filter length (Becker 2016). The more control lines are planned, the more crossover points arise and the more reliable is a statement on the precision of the results.

In airborne gravimetry, the accuracy of the estimated gravity is usually determined as the root mean square (RMS) of the residuals at all redundant points (e. g. Glennie and Schwarz 1999, Ayres-Sampaio et al. 2015, Becker 2016). If the measurement accuracy can be considered equal for both line traversals, the standard deviation is obtained by dividing the RMS by $\sqrt{2}$ (e. g. Glennie and Schwarz 1999). The resulting value is also called "RMS error" (RMSE, e. g. Forsberg and Olesen 2010, Becker 2016).

6.2 Crossover Adjustment

In section 5.1, a bias and a linear drift per flight have already been removed from the gravity disturbance estimates. The impact of remaining non-linear drifts and other long-wavelength errors can be reduced by performing a crossover adjustment, also known as "crossover leveling". The assumption that the gravity disturbance is equal at the crossover points of two crossing flight lines can be used to determine one bias for each line. These line biases can be estimated using a least-squares adjustment, e. g. a Gauß Markov Model based on the assumption that the crossover residuals are equal to the difference of the line biases of the two corresponding lines, plus additional white noise. To avoid a rank deficiency in the adjustment, an additional pseudo observation is added to anchor the model, e. g. requiring that the sum of all biases equals zero.

For any flight line to be included in the adjustment, at least two valid crossover points have to be present on this line. A crossover point is regarded as valid, if both of its adjacent lines have a sufficient number of crossover points. If a line with only one crossover point was included in the adjustment, its adjusted crossover residual is necessarily zero, leading to overoptimistic statistics.

If the number of crossover points is low, there is a risk of over-parametrization leading to less reliable results and in general to a too optimistic RMS/RMSE (Becker 2016). Then, the adjusted line network is susceptible to distortion and an adjustment is not always recommended. If an adjustment is performed nevertheless, a correction factor ρ_i can be introduced in order to produce more realistic overall statistics: The residuals are multiplied with a correction factor ρ_i, which has to be determined for every flight line i depending on the line's particular number n_i of crossover points. Using the Gamma function $\Gamma(x)$, correction factors for the crossover residuals can be determined with the analytic function (Becker 2016)

$$\rho_i(n_i) = \sqrt{\frac{n_i - 1}{2}} \cdot \frac{\Gamma\left(\frac{n_i - 1}{2}\right)}{\Gamma\left(\frac{n_i}{2}\right)}. \tag{15}$$

The adjusted crossover residuals are multiplied with the mean of the correction factors of the two adjacent lines, respectively. For $n_i = 2(3)$ points adjacent to a line, $\rho_i = 1.25(1.13)$. For a large number of crossover points,

the correction factor converges to one and becomes negligible.

If there are long flight lines with plenty of crossover points, a linear drift could be estimated in addition to the bias for each flight line (Hwang et al. 2006). In the scope of this paper, the adjustment was limited to line biases only.

7 A Case Study

7.1 Sensors and Data

The measurements have been conducted with an inertial measurement unit (IMU) of the type iNAV-RQH-1003 by iMAR (Fig. 3). This IMU comprises of a triad of Honeywell QA-2000 accelerometers and a triad of Honeywell GG1320A ring laser gyroscopes. For further information

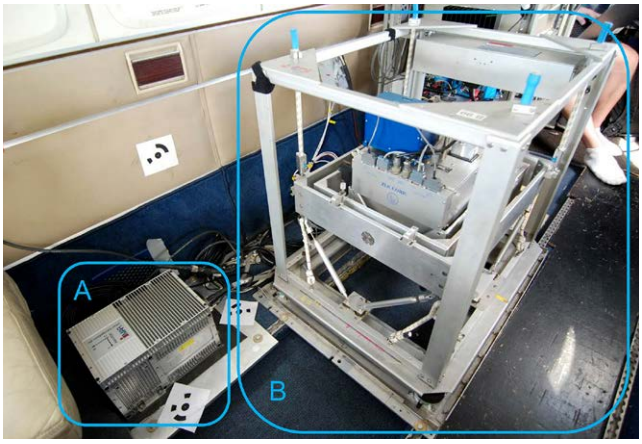

Fig. 3: iMAR iNAV-RQH-1003 (A) and horizontally stabilized LaCoste and Romberg S-gravimeter (B)

on the IMU and manufacturer's data, the reader is referred to Becker (2016) and IMAR Navigation (2012). Previous research has shown that with this IMU, results consistent at the 2-mGal level in comparison to a stable-platform LaCoste and Romberg S-gravimeter are possible, if a simple warm-up calibration of the vertically aligned accelerometer is applied as described in section 5.3.

In order to evaluate the direct method presented in sections 4 and 5, data of an airborne gravity campaign conducted in Malaysia in 2014 are evaluated. The flights were undertaken from Kota Kinabalu Airport in Borneo's north. Most of the 12 flights were flown in a north-westerly direction above the South China Sea. With a line spacing of 10 km for the offshore and 5 km for the coastal flights, an area of about 68,000 km^2 was covered. The flights were performed in auto pilot mode with a twin-engine propeller aircraft of the type Beechcraft King Air 350. The mean velocity was 88 m/s and the mean altitude 1.9 km. The cumulative flight distance is nearly 13,000 km. IMU data is available at a frequency of 300 Hz, GNSS data with 5 Hz.

In this work, the direct method has been implemented as follows: First, the commercial software NovAtel Waypoint GrafNav 8.60 (NovAtel Inc. 2014a) was used to produce GNSS position solutions by Precise Point Positioning (PPP). The GNSS/IMU integration was performed using NovAtel Waypoint Inertial Explorer 8.60 (NovAtel Inc. 2014b) to obtain precise attitude angles. Second, a MATLAB software has been developed at the chair of Physical and Satellite Geodesy at the Technical University of Darmstadt, implementing the IMU pre-processing, numerical differentiation of the GNSS positions, Eötvös correction, low-pass filtering and the corrections as presented in section 5. The full set of corrections described in the scope of this paper have been applied, including the crossover correction factors ρ_i.

The gravity disturbance estimates are filtered using a finite impulse response (FIR) low-pass filter with a filter length of 130 s (corresponding to the inverse of the –6 dB cutoff frequency, designed with the window method). The selection of the IMU acceleration filter is less critical than the gravity disturbance filter. Hence, for efficiency reasons, an infinite impulse response Butterworth filter (IIR) and a filter length of 1.6 s have been designed as IMU acceleration low-pass filter. For details on these filter types see, e. g., von Grünigen (2014). The empirical selection of the filter lengths depends on IMU sensor characteristics, flight dynamics, etc.

7.2 Results

The gravity disturbance estimates are shown in Fig. 4. The gravity estimates correlate well with features in the seafloor topography. About 100 crossover points have been identified. Fig. 5 shows the distribution of the crossover residuals, arranged per flight line. The absolute values of all residuals are smaller than 6 mGal. After crossover adjustment, per-line biases are removed from the results

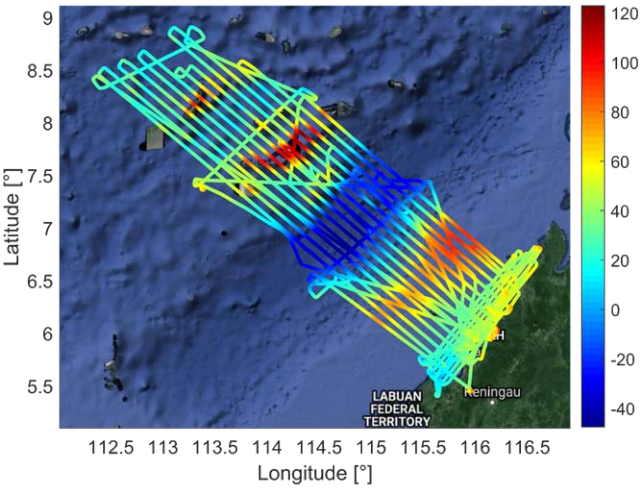

Fig. 4: Gravity disturbance (down component) [mGal] along flight trajectories north-west of Borneo without adjustment (Map data: Google, Landsat/Copernicus)

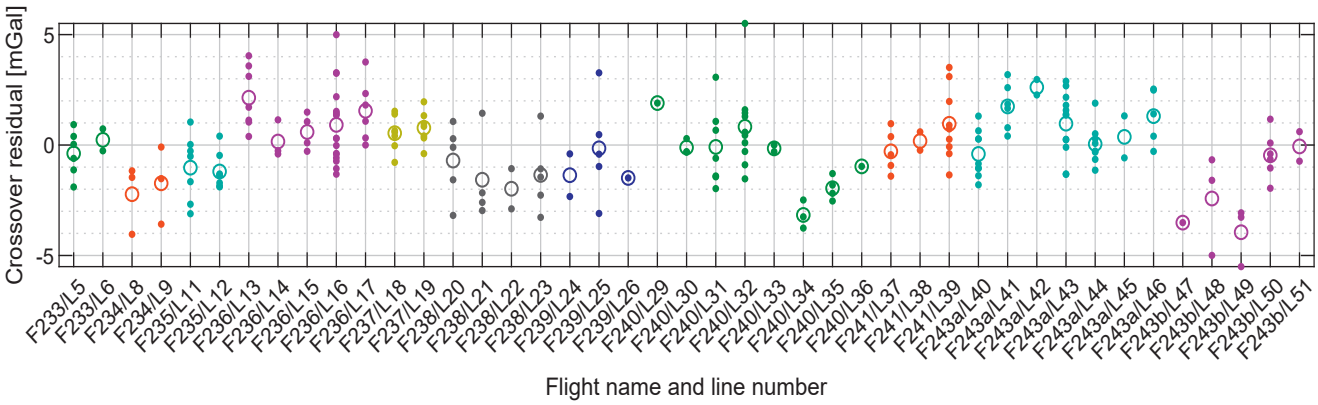

Fig. 5: Vertical residuals of the crossover points without adjustment, sorted by flights and flight lines, with mean residuals (annuluses)

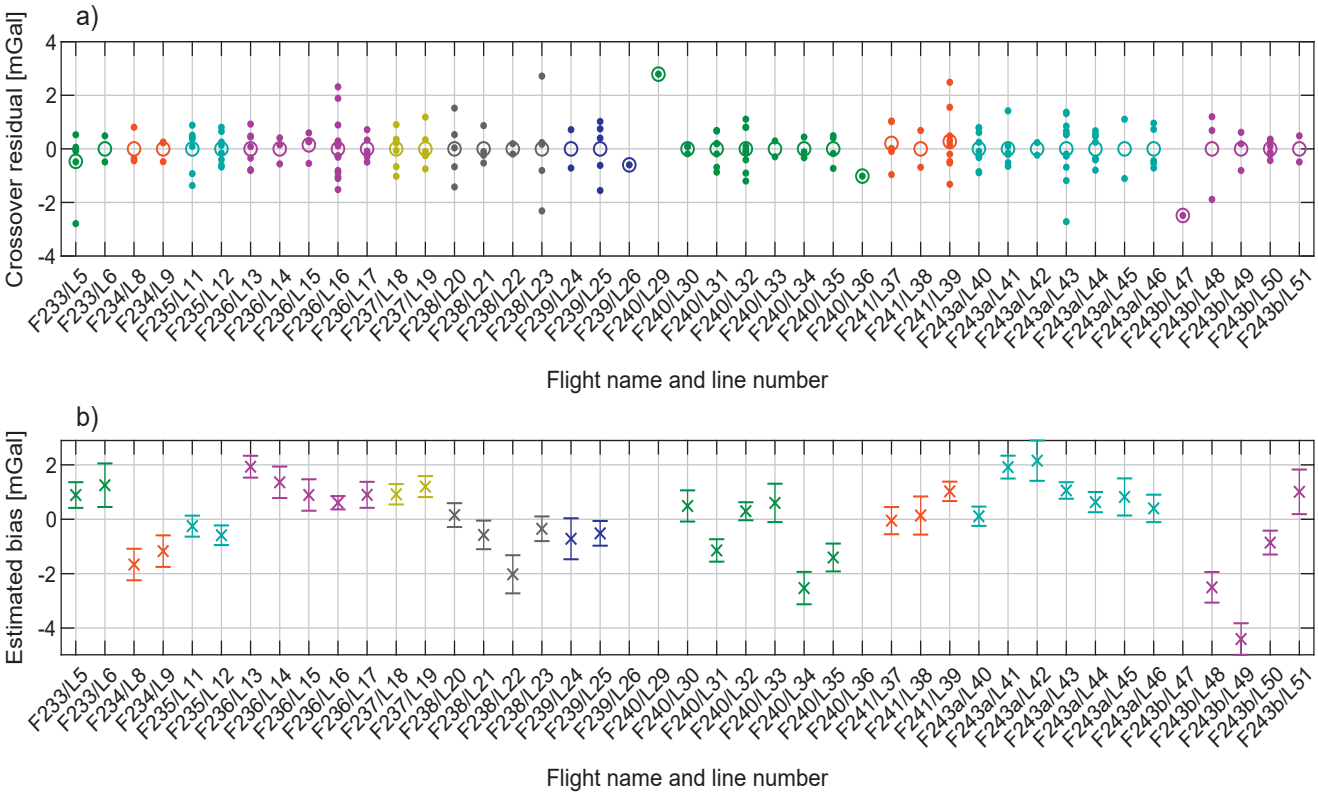

Fig. 6: a) Vertical residuals of the adjusted crossover points by flights and flight lines, with mean residuals (circles); b) Estimated vertical biases of the flight lines with their estimated standard deviations

leading to smaller residuals within ±3 mGal. The adjusted residuals are plotted in Fig. 6a, including lines with less than two crossover points, which were excluded from the adjustment. Fig. 6b shows the estimated line biases and their corresponding standard deviations.

The resulting crossover residual standard deviations (RMSE) are noted in Tab. 1. The results of the indirect method are taken from (Becker 2016). The overall accuracy is on a par for both the non-adjusted (1.3 mGal) and adjusted results (0.6 … 0.7 mGal). For an average survey flight, the gravity disturbance differences between the two methods are shown in Fig. 7.

Tab. 1: RMSE of crossover residuals of the vertical gravity disturbance component (in mGal); correction factors (cf. equation (15)) were applied to the adjusted results; right column: RMSE of the differences between the direct and the indirect methods, for the non-adjusted gravity estimates

Method	Not adjusted	Adjusted	Difference direct/indirect
Direct	1.26	0.62	0.82
Indirect	1.30	0.68	

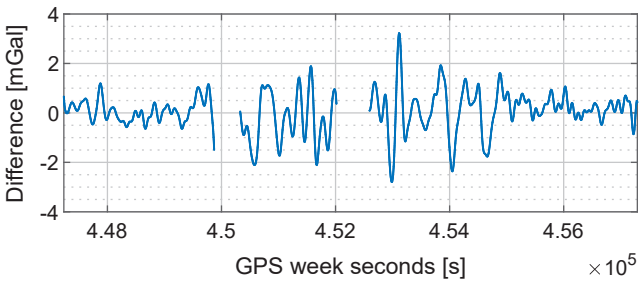

Fig. 7: Flight number 241: Vertical difference between the direct and the indirect method (only showing survey lines)

In consideration of the flight velocity and the cut-off filter length, the spatial resolution of the direct method is about 6 km (half wavelength). Using the indirect method, there is no explicit spatial or temporal gravity resolution parameter since the Kalman filter operates as a low-pass filter. Instead, the campaign-wide settings for the stochastic process parameters describing the along-flight gravity variations were tuned to minimize the crossover residuals. The resulting spatial resolution of approximately 130 s full wavelength (6 km half-wavelength) is similar as for the direct method.

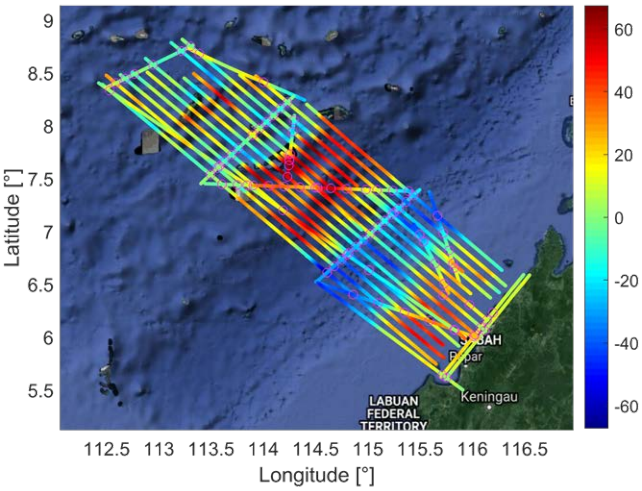

Fig. 8: Gravity disturbance (north component) [mGal] after adjustment (Map data: Google, Landsat/Copernicus)

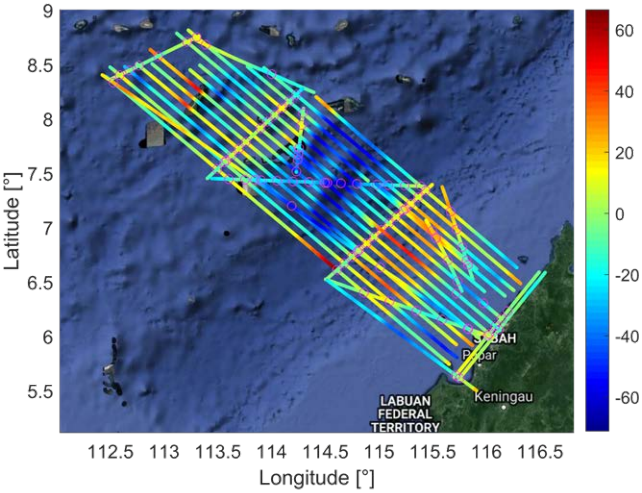

Fig. 9: Gravity disturbance (east component) [mGal] after adjustment (Map data: Google, Landsat/Copernicus)

In general, when comparing overall statistics among different campaigns or scientific publications, the flight conditions, terrain properties, the processing approach and parameters have to be taken into account.

All accuracy values mentioned above are based on the same measurements. In order to get a measure for the external accuracy, Becker (2016) compared the results of the indirect method to the GGM05C global gravity model (Ries et al. 2016). The mean difference is smaller than 1.2 mGal if the simple thermal correction is applied to the vertical accelerometer. For this comparison, a quasi-regular grid of comparison points was used, with a grid spacing of about 20 km.

Due to the greater impact of attitude errors on the horizontal gravity components (Becker et al. 2015a), only the adjusted data allow meaningful results for these components. First results are illustrated in Fig. 8 and Fig. 9. For both components, an RMSE of about 8 mGal is obtained, which corresponds to 1.7 arc seconds if expressed as deflections of the vertical. A detailed examination of these deflections is subject to further research.

8 Conclusions and Outlook

In this paper, an algorithm for the direct evaluation method of airborne strapdown gravimetry has been presented and the results have been compared to results obtained with the indirect method using the same data set. An accuracy of 1 to 2 mGal has been obtained at flight altitude even without crossover adjustment if a simple thermal correction is applied to the vertical accelerometer readings. Based on the crossover residuals, a standard deviation of 1.26 mGal has been reached, being comparable to the indirect method (1.3 mGal) on the same data set. After a crossover adjustment was applied, a standard deviation of 0.62 mGal was obtained for the direct method being slightly better than the indirect method with 0.68 mGal. The spatial resolution is about 6 km (half-wavelength).

It is just noted here, that also for a similar gravimetry campaign, carried out in Mozambique and Malawi in 2015 (Becker et al. 2016), both methods produced equal accuracy levels. The two methods might be further compared investigating high-turbulence scenarios or campaigns without autopilot usage.

The attitude determination with a commercial software facilitates the implementation of the direct method, but details on the attitude determination are hidden in a “black box”. Nevertheless, since the implementation of the direct method is more straightforward than the set-up of the Kalman filter based indirect method, the direct method has been shown to be a useful alternative, avoiding the delicate Kalman filter tuning of the indirect method.

There are possible improvements to the direct procedure as described in this paper: For example, the parameters of the GNSS/IMU integration might be optimized. Further, the gravity disturbance low-pass filter might be optimized in order to avoid boundary effects at the edges of the flight lines.

Acknowledgements

The financial support by the Deutsche Forschungsgemeinschaft (DFG) as a part of the project "Innovative calibration methods for strapdown airborne vector gravimetry aboard HALO" within the framework of SPP 1294 "Atmospheric and Earth System Research with the "High Altitude and Long Range Research Aircraft" (HALO)" is gratefully acknowledged. The Malaysia airborne gravity campaign was financed by the Department of Survey and Mapping, Malaysia (JUPEM) and was conducted in cooperation with the Technical University of Denmark (DTU Space).

References

Ayres-Sampaio, D., Deurloo, R., Bos, M., Magalhães, A., Bastos, L. (2015): A Comparison Between Three IMUs for Strapdown Airborne Gravimetry. In: Surveys in Geophysics. DOI: 10.1007/s10712-015-9323-5.

Becker, D. (2016): Advanced Calibration Methods for Strapdown Airborne Gravimetry. Technische Universität Darmstadt. Available from: http://tuprints.ulb.tu-darmstadt.de/5691.

Becker, D., Becker, M., Leinen, S., Zhao, Y. (2015a): Estimability in strapdown airborne vector gravimetry. In: International Association of Geodesy Symposia. DOI: 10.1007/1345_2015_209.

Becker, D., Becker, M., Olesen, A.V., Nielsen, J.E., Forsberg, R. (2016): Latest results in strapdown airborne gravimetry using an iMAR RQH unit. In: 4th IAG symposium on Terrestrial Gravimetry. State Research Center of the Russian Federation, 19–25.

Becker, D., Nielsen, J.E., Ayres-Sampaio, D., Forsberg, R., Becker, M., Bastos, L. (2015b): Drift reduction in strapdown airborne gravimetry using a simple thermal correction. In: Journal of Geodesy 89: 1133–1144. DOI: 10.1007/s00190-015-0839-8.

Becker, M., Hehl, K. (2012): Geodäsie. WBG, Darmstadt.

Brozena, J.M., Peters, M.F., Salman, R. (1997): Arctic Airborne Gravity Measurement Program. In: Segawa, J,. Fujimoto, H., Okubo, S. (Eds,): Gravity, Geoid and Marine Geodesy. Springer. Berlin, Heidelberg. DOI: 10.1007/978-3-662-03482-8_20.

Forsberg, R., Olesen, A.V. (2010): Airborne gravity field determination. In: Xu, G. (Ed.): Sciences of Geodesy – I: Advances and Future Directions. Springer. Berlin. 83–104. DOI: 10.1007/978-3-642-11741-1_3.

Glennie, C.L., Schwarz, K.P. (1999): A comparison and analysis of airborne gravimetry results from two strapdown inertial/DGPS systems. In: Journal of Geodesy: 311–321. DOI: 10.1007/s001900050248.

Glennie, C.L., Schwarz, K.P., Bruton, A.M., Forsberg, R., Olesen, A.V., Keller, K. (2000): A comparison of stable platform and strapdown airborne gravity. In: Journal of Geodesy 74: 383–389. DOI: 10.1007/s001900000082.

Groves, P.D. (2013): Principles of GNSS, inertial and multisensor integrated navigation systems. 2nd ed. Artech House. Boston, London.

von Grünigen, D.C. (2014): Digitalfilter. 5th ed. Hanser, Leipzig.

Hwang, C., Hsiao, Y.S., Shih, H.C. (2006): Data reduction in scalar airborne gravimetry: Theory, software and case study in Taiwan. In: Computers and Geosciences: 1573–1584. DOI: 10.1016/j.cageo.2006.02.015.

IMAR Navigation (2012): Inertial Measurement System for Advanced Applications. St. Ingbert. Available from: www.imar-navigation.de/downloads/NAV_RQH_1003_en.pdf.

Jekeli, C. (2001): Inertial Navigation Systems with Geodetic Applications Inertial Navigation Systems with Geodetic Applications. Berlin.

Jekeli, C., Garcia, R. (1997): GPS phase accelerations for moving-base vector gravimetry. In: Journal of Geodesy 71: 630–639. DOI: 10.1007/s001900050130.

Kwon, J.H., Jekeli, C. (2001): A new approach for airborne vector gravimetry using GPS/INS. In: Journal of Geodesy 74: 690–700. DOI: 10.1007/s001900000130.

Li, M., Xu, T., Lu, B., He, K. (2019): Multi-GNSS precise orbit positioning for airborne gravimetry over Antarctica. In: GPS Solutions 23: 53. DOI: 10.1007/s10291-019-0848-9.

Moritz, H. (1980): Geodetic reference system 1980. In: Bulletin Géodésique. DOI: 10.1007/BF02521480.

Nettleton, L.L., LaCoste, L., Harrison, J.C. (1960): Tests of an Airborne Gravity Meter. In: Geophysics 25. DOI: 10.1190/1.1438685.

NovAtel Inc. (2014a): GrafNav/GrafNet 8.60 User Guide. Available from: www.novatel.com/support/info/documents/572.

NovAtel Inc. (2014b): Inertial Explorer® 8.60 User Guide. Available from: www.novatel.com/support/info/documents/572.

Ries, J., Bettadpur, S., Eanes, R., Kang, Z., Ko, U., McCullough, C., Nagel, P., Pie, N., Poole, S., Richter, T., Save, H., Tapley, B. (2016): The Combination Global Gravity Model GGM05C. DOI: 10.5880/icgem.2016.00.

Salazar, D., Hernandez-Pajares, M., Juan-Zornoza, J.M., Sanz-Subirana, J., Aragon-Angel, A. (2011): EVA: GPS-based extended velocity and acceleration determination. In: Journal of Geodesy 85: 329–340. DOI: 10.1007/s00190-010-0439-6.

Schwarz, H.R., Köckler, N. (2011): Numerische Mathematik. 8th ed. Vieweg+Teubner, Wiesbaden. DOI: 10.1007/978-3-8348-8166-3.

Torge, W., Müller, J. (2012): Geodesy. 4th ed. de Gruyter. Berlin, Boston.

Wei, M., Schwarz, K.P. (1998): Flight test results from a strapdown airborne gravity system. In: Journal of Geodesy: 323–332. DOI: 10.1007/s001900050171.

Zhang, X., Zheng, K., Lu, C., Wan, J., Liu, Z., Ren, X. (2017): Acceleration estimation using a single GPS receiver for airborne scalar gravimetry. In: Advances in Space Research: 2277–2288. DOI: 10.1016/j.asr.2017.08.038.

Contact

Felix Johann, M.Sc. | Prof. Dr.-Ing. Matthias Becker
Physikalische Geodäsie und Satellitengeodäsie
Technische Universität Darmstadt
Franziska-Braun-Straße 7, 64287 Darmstadt
johann@psg.tu-darmstadt.de | becker@psg.tu-darmstadt.de

Dr.-Ing. David Becker
School of Earth and Planetary Sciences
Curtin University
Kent Street, Perth, Western Australia 6102
david.becker@curtin.edu.au

Prof. René Forsberg
National Space Institute
Technical University of Denmark
Elektrovej, 2800 Kgs. Lyngby/Denmark
rf@space.dtu.dk

Dr. Majid Kadir
Info-Geomatik
72 Jalan Pendidikan 4, 81300 Skudai
Taman Universiti, Johor/Malaysia
igeom2006@gmail.com

This article also is digitally available under www.geodaesie.info.